

## Simulation study of the energy distributions of the hadron, muon, all charged and electromagnetic EAS components on Mt. Aragads Altitude

J.-N. Capdevielle<sup>1</sup> and Kh. N. Sanosyan<sup>2</sup>

<sup>1</sup>Laboratoire de Physique Corpusculaire et Cosmologie, Collège de France, 11 pl. Marcelin Berthelot, F 75231 Paris,, Cedex 05, FRANCE

<sup>2</sup>Cosmic Rays' Department, Yerevan Physics Institute, Alikhanyan Brothers' St. 2, 375036 Yerevan, ARMENIA

**Abstract.** The energy dependences of densities of gammas, electrons, muons, hadrons and all charged particles as well as the energy distributions of these components of EAS for both primary protons and iron nuclei are presented for the observation level of the Cosmic Ray Station on Mt. Aragads (3200m a.s.l.) in the energy interval  $1.5 \cdot 10^5 \div 1.5 \cdot 10^7$  GeV.

### 1 Introduction

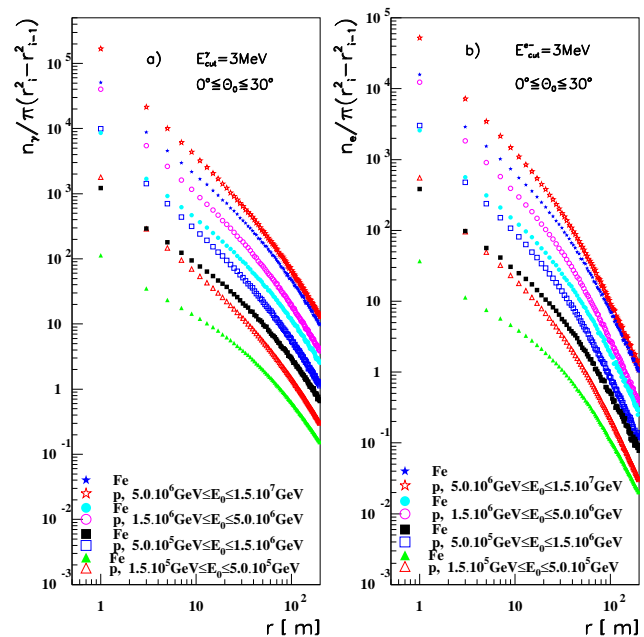
A thorough understanding, analyses in terms of EAS observables and even some calibration procedures of the data accumulated with the detector facilities (Chilingarian et al. , 1999; Hovsepyan et al. , 1999) operated in the ANI Cosmic Ray Laboratory on Mt. Aragads, Armenia, require the comparison with realistic Monte-Carlo calculations for the case of the ANI observation level (3200m a.s.l., latitude:  $N40.47^\circ$  longitude:  $E44.18^\circ$  allowing a detailed study of various shower variables and of their correlations. The results of the analysis of the simulated lateral distributions of various EAS components are communicated detailed in our earlier paper (Capdevielle and Sanosyan, 1999).

### 2 Simulation procedures

The EAS simulation used the Monte Carlo code CORSIKA (version 5.62) (Capdevielle et al. , 1992; Heck et al. , 1998) for calculating proton and iron induced showers for four different energy intervals:  $(1.5-5.0) \cdot 10^5$  GeV,  $5.0 \cdot 10^5$  GeV –  $1.5 \cdot 10^6$  GeV,  $(1.5-5.0) \cdot 10^6$  GeV, and  $5.0 \cdot 10^6$  GeV –  $1.5 \cdot 10^7$  GeV.

As generator of the high energy hadronic interactions the option of the QGSJET model (Kalmykov et al. , 1997) has been chosen, while for the low energies the GHEISHA model has been invoked. The electromagnetic component is treated

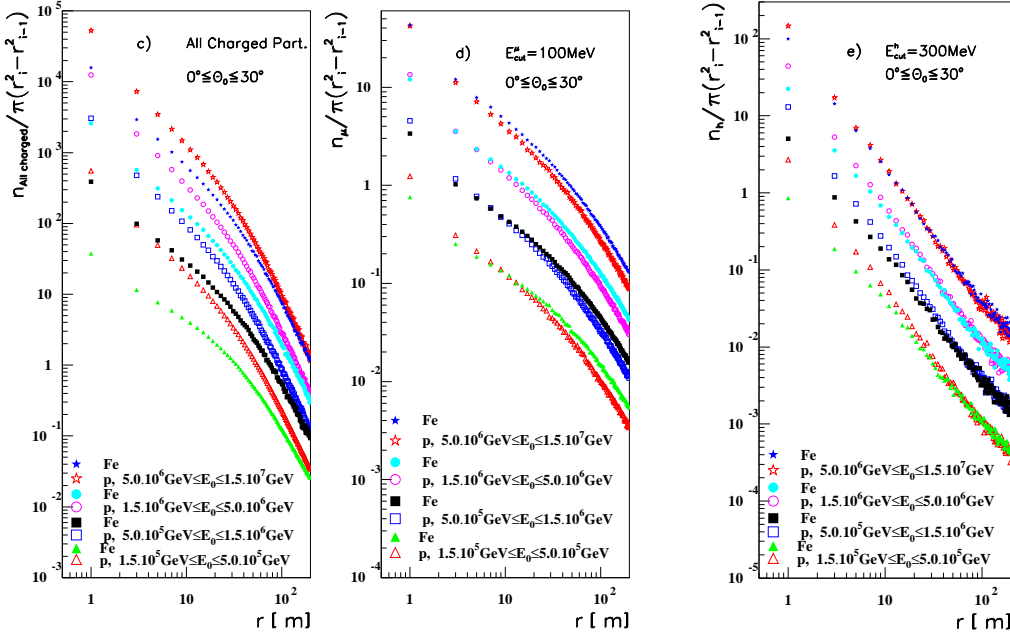
Correspondence to: J.-N. Capdevielle  
(capdev@cdf.in2p3.fr)



with the NKG approximation as well as optionally with the EGS4 procedure. In the latter case a thinning procedure (Hillas, 1997) has been applied with the thinning factor  $10^{-4}$  for last three energy intervals. Effects due to thinning have been controlled by comparative calculations without thinning for the first energy interval. Particles have been stored with energy thresholds above 0.3 GeV for hadrons, 0.1 GeV for muons and 3 MeV for electrons and gamma rays.

For the determination of the lateral energy distributions of the muons we consider also two different muon energy thresholds of 2.5 GeV and 5 GeV. Within one bin of the primary energy the energy has been randomly chosen along the power law dependence of the spectrum with the spectral index of  $\gamma = -2.7$ . Similarly the angle of incidence is selected from the interval  $[0^\circ - 30^\circ]$  in a way so that isotropic incidence is guaranteed.

It appears very crucial to take into account the effects of



the magnetic field of the Earth. Introducing the coordinates of the Mt. Aragads station, the magnetic field components have been calculated by the Geomagnetic Field Synthesis Program (Version 3.0) (NGDC-NOAA , 1998) with the results (1999): magnetic declination: 4d 41.1m, horizontal component: 25157nT, vertical component: 41215nT.

### 3 Densities of shower main components

The energy dependences of the densities of shower main components at observation level are displayed by normalized lateral distributions in Figure 1. The densities of gammas, electrons, all charged particles, muons, and hadrons are presented in figures a), b), c), d), and e) respectively. The bold symbols in all figures correspond to the iron primary while the empty symbols represent the proton primary. Figure 1 shows that some changes in the slope of the densities with energy is obvious, but also with the type of the primary. For gammas, electron-positron, and all charged particles there appear "crossings tendency" of the lateral density distributions at large ( $> 200m$ ) radii for iron and proton induced showers. For muon densities the "crossing" occurs at  $\approx 11m$  from shower core for the lowest energy interval and just at  $\approx 1m$  from the axis for the highest energy interval. For hadron densities the "crossing" point moves from  $\approx 10m$  up to  $200m$  with increase of energy. One interesting conformity with a law is visible in Figure 1 for all particle types and for all energy intervals. It is the refraction of all curves at almost the same region 30-40m of the distance from shower axis. This persistence can become more convincing if the same dependences will be presented in an other scale by multiplying the density values by a factor that will flatten a part of the curve and the next part will demonstrate the refraction. In this case one have to consider this regularity taking into account the

**Fig. 1.** Energy dependences of densities of gammas -a), electron-positrons -b), all charged particles -c), muons -d), and hadrons -e) for proton and iron primaries of various energies.

behaviour of the shower age parameter before and after 35m from shower core.

### 4 Energy distributions for proton and iron nucleus induced showers.

Related to the studies of the energy distributions of above mentioned EAS components is the question of the dependence of the simulated EAS pattern from the hadronic interaction models, used as generators of the Monte-Carlo simulation (ANI Workshop , 1999). In this aspect to study the energy distributions of shower components in the complex for the same simulation will give more integrant picture of EAS development, and allows to make more realistic inferences in the framework of QGSJET model which we have used.

Aiming this goal proton and iron induced showers in the atmosphere are simulated in four energy intervals between the mentioned region by the help of CORSIKA code. The energy distributions of muons for both primary protons and iron nuclei are presented. The methodological procedure of the present CORSIKA simulation is described in detail in our earlier work (Capdevielle and Sanosyan, 1999).

#### 4.1 Muon energy distribution.

We have calculated the energy distribution of muons with threshold energies of  $2.5GeV$  and  $5GeV$  with which the muons are registered by GAMMA facility in Aragads high altitude cosmic ray station.

The energy distributions of muons at  $700g/cm^2$  observation

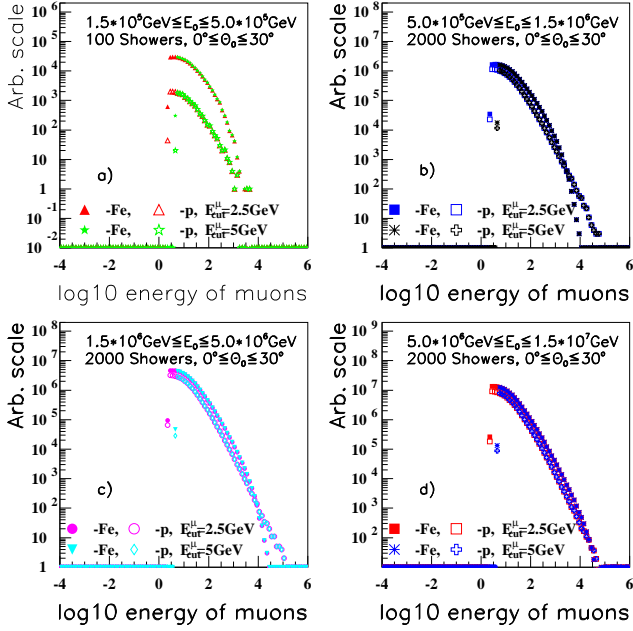


**Fig. 2.** Muons energy distribution for proton and iron nuclei induced showers for four energy intervals with 2.5 and 5 GeV muon cutoff energies.

level are displayed in Figure 2. The distributions for four primary energy intervals  $(1.5 \div 5.0) \times 10^5 \text{ GeV}$ ,  $5.0 \times 10^5 \div 1.5 \times 10^6 \text{ GeV}$ ,  $(1.5 \div 5.0) \times 10^6 \text{ GeV}$ , and  $5.0 \times 10^6 \div 1.5 \times 10^7 \text{ GeV}$  are presented in figures a), b), c), and d) respectively. The bold symbols in all figures here and after correspond to the iron primary while the empty symbols represent the proton primary. Figure 2 shows that the energy distribution for both thresholds is almost the same for the same primary particle after the maximum of the curve while before the maximum the distribution for 2.5 GeV is a little bit higher and reaches to its maximum earlier. This significance is present both for proton and iron primaries for all energy intervals. From the Figure 2 it is obvious also the type dependence of energy distribution which is more noticeable for the lower energy interval (see Figure 2. a)). Iron induced showers have higher muon energy distribution than proton induced showers, and for the first primary energy interval this abundance of low energy muons in iron induced showers exceeds those of for proton induced showers more than one order. But there is an intersection of this curves at the value of abscissa equal to 3, 3.5, 4, and 4.5 (see Figure 2. a), b), c), and d) respectively). The primary particle type dependence decrease with the increasing of primary energy and almost disappears in the fourth energy interval (see Figure 2. d)). The same distributions for muons energy threshold 100 MeV are presented in Figure 3. One can see total agreement between the figures for b), c), and d) energy intervals with the obvious energy expansion towards the direction of low energies up to 100 MeV. As for the lowest energy interval for the case  $E_{cut}^\mu = 100 \text{ MeV}$  the muons energy distribution for proton showers almost reaches to those for iron showers. In this case

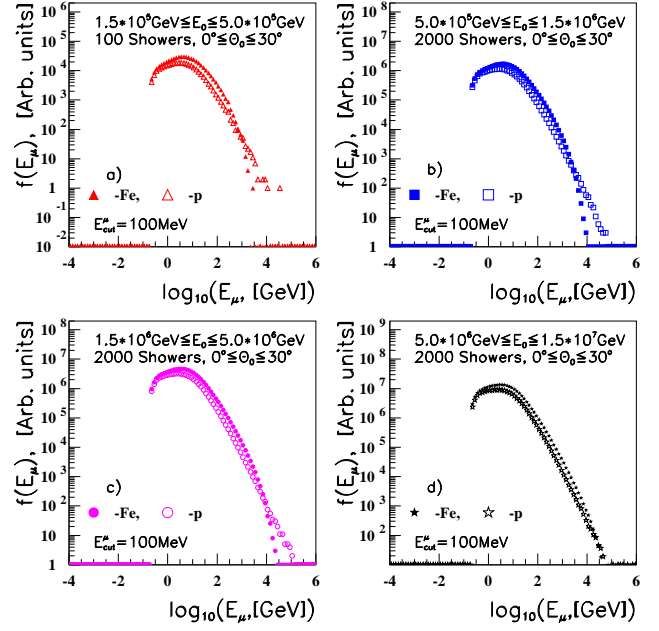


**Fig. 3.** Muons energy distribution for proton and iron nuclei induced showers for four energy intervals with muon energy threshold equal to the input value (100 MeV).

also the intersection point of two curves remains the same  $\log_{10} E_\mu \approx 3$ .

#### 4.2 Photons energy distribution.

The energy distributions of photons at relevant observation level and in referred four energy ranges are demonstrated in Figure 4 for different primaries. The results demonstrated in Figure 4 indicate in general differences with the case of muons energy distribution for all energy intervals. In this case the intersections of iron induced shower photons distributions curves with those of proton induced shower curves do not take place because for all energy intervals the proton induced shower curves are higher than the energy distribution curves for iron induced showers, although the photons energy distribution curves for these energy intervals also have slow expressed refraction at the abscissa values 1.5, 2, 2.5, and 3 (see Fig. 4. a), b), c), and d) respectively).

It worths to say that if one will try to plot the same distributions by applying the 2.5/5 GeV threshold rejection on original distributions then for the first primary energy interval one will receive a place exchanged picture for the curves of proton and iron induced showers, i.e. the iron showers photon distribution will lie higher than protons one.

An other quantitative difference from the muons distribution is that the intensity of the flux of the photons is approximately 100 times higher with proportion those of muons flux for the same energy bins for all four energy regions.

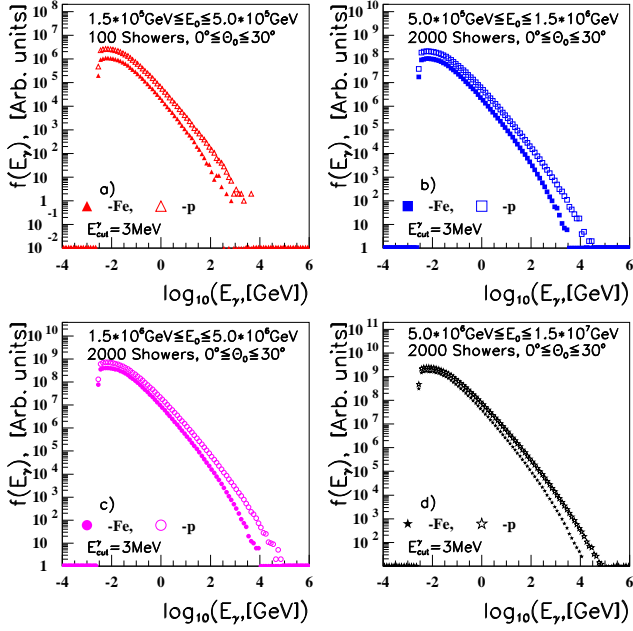


**Fig. 4.** Photons energy distribution for proton and iron nuclei induced showers for four energy intervals.

#### 4.3 Electrons energy distribution.

The next electromagnetic component is presented in Figure 5. The graph shows the energy distributions of electrons for the same showers object of curiosity. The results for this case corroborates the common behaviors of electron component in the total electromagnetic proportion of the cascade, i.e. the electrons energy distribution repeats in all aspects the gammas energy distribution (Fig. 4) with the  $\sim 6$  decreasing factor.

#### 4.4 Hadrons energy distribution.

Hadron energy distribution will be reported during the conference.

#### 4.5 Converted energy distributions.

In the primary energy interval  $(1.5 - 5.0) \cdot 10^6 \text{ GeV}$  the observation of "knee" in all EAS components has been considered as an indication that the kink is of astrophysical origin (Haungs et al., 1999). Converting the different energy spectra, following the procedure:

$$dN/dE \rightarrow (dN/dE) \cdot \langle E \rangle^{2.7}, \quad (1)$$

where  $\langle E \rangle$  is the energy mean value in a bin, we derived from the electron energy spectra the primary spectrum displayed on Figure 6.

Figure 6 shows that the energy spectrum of secondary electrons in proton induced showers have not any refraction while the same distribution for those of iron nuclei generated cascade has a well expressed "knee" at  $10^3 \text{ GeV}$ .

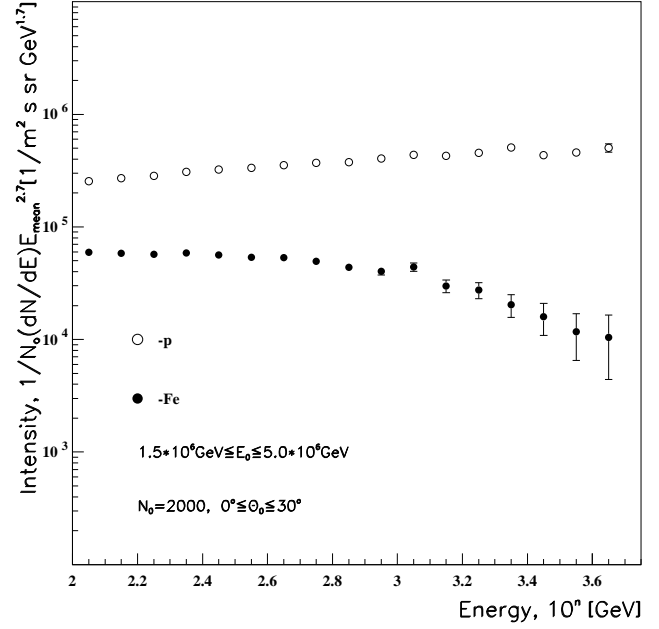


**Fig. 5.** Electrons energy distribution for proton and iron nuclei induced showers for four energy intervals.

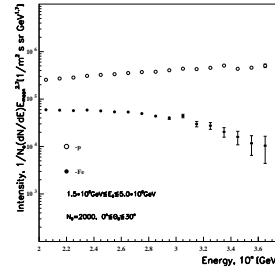


**Fig. 6.** The converted energy distribution of electrons.

## References

- Chilingaryan, A. et al., Proc. ANI Workshop 1999, Report FZKA 6472, 91-94, Karlsruhe, 2000.
- Eganov, V.S. et al., ibidem, 87-90.
- Blokhin, S.V., Romakhin, V.A., and Hovsepian, G.G., Proc. ANI Workshop 1999, Report FZKA 6472, 111-114, Karlsruhe, 2000.
- Chilingaryan, A. et al., ibidem, 53-58.
- Capdevielle, J.-N. and Sanosyan, Kh.N., Proc. ANI Workshop 1999, Report FZKA 6472, 75-82, Karlsruhe, 2000.
- Capdevielle, J.-N. et al., Report KfK 4998, Karlsruhe, 1992.
- Heck, D. et al., Report FZKA 6019, Karlsruhe, 1998.
- Kalmykov, N.N., Ostapchenko, S.S., and Pavlov, A.I., Nucl. Phys. B (Proc. Suppl.) **52B** 17, 1997.
- Hillas, A.M., Nucl. Phys. B (Proc. Suppl.) **52B** 29, 1997.
- Geomagnetic Field Synthesis Program, 1998: <http://www.ngdc.noaa.gov/seg/potfld/>
- Editors: Chilingarian, A.A., Haungs, A., Rebel, H., Sanosyan, Kh.N., Proc. ANI Workshop 1999, Report FZKA 6472, iii, Karlsruhe, 2000.
- Haungs, A. et al., Proc. ANI Workshop 1999, Report FZKA 6472, 31-42, Karlsruhe, 2000.